Log-Linear Models, Extensions and Applications

Editors:

Aleksandr Aravkin saravkin@us.ibm.com
IBM T.J. Watson Research Center
Yorktown Heights, NY 10589

Anna Choromanska achoroma@cims.nyu.edu
Courant Institute, NYU
New York, NY

Li Deng deng@microsoft.com
Microsoft Research
Redmond, WA 98052

Georg Heigold heigold@google.com
Google Research
Mountain View, CA 94043

Tony Jebara jebara@cs.columbia.edu
Columbia University
NYC, NY 10027

Dimitri Kanevski dkanevski@google.com
Google Research
NYC, NY 10011

Stephen J. Wright swright@cs.uwisc.edu
University of Wisconsin
Madison, WI 53706

The MIT Press
Cambridge, Massachusetts
London, England

Contents

1 Informative Nonstationarity in Paleoclimatological Loglinear Models

Yuriy S. Polyakov polyakov@njit.edu
New Jersey Institute of Technology
Newark, New Jersey

Fabrice Lambert lambert@uc.cl
Department of Physical Geography, Catholic University of Chile
Santiago, Chile

Serge F. Timashev serget@mail.ru
Karpov Institute of Physical Chemistry, Moscow, Russia
Troitsk, Moscow Region, Russia

We examine the relation between temperature and logarithmized dust flux from the EPICA Dome C ice core (Antarctica) for the last 800,000 years. Our focus is on the nonstationarity analysis of dust flux time series rather than the regression analysis of correlations between temperature and dust flux (conventional method in paleoclimatology). The analysis is performed using flicker-noise spectroscopy, a phenomenological statistical physics framework developed for the analysis of natural signals with stochastically varying components. Our study shows that the logarithmized dust flux time series is statistically nonstationary. It contains alternating intervals of quiescence and high activity. The quiescent intervals appear to be related to glacial conditions in the temperature series. The periods of high activity appear to correspond to warming events, potentially leading to interglacial conditions. These results can be used to explain why significant correlations between temperature and dust flux exist in the glacial conditions and why there is virtually no correlation during interglacial periods.

1.1 Introduction

Paleoclimatology deals with the analysis of climate change on the scale of Earth's entire history. The records for past climate are reconstructed indirectly based on the "proxy" data acquired from paleoclimatic archives, such as ice cores, tree rings, and marine sediment cores. The correlations between the proxy data for modern age and recent climate records are used to build mathematical models that can be applied to infer past climate using the proxy data for the time period of interest. This procedure generally involves a large number of factors with complex interactions and feedback loops.

One of major factors studied in paleoclimatology is the aerosol load of the atmosphere. Mineral dust aerosols are generally emitted from deserts, and their small-sized fractions can travel to distant areas, for example polar regions. This enables paleoclimatologists to examine the dust content in ice cores from polar regions and draw conclusions about atmospheric processes on a global scale. In this study, we examine data from the European Project for Ice Coring in Antarctica (EPICA) Dome C ice core located on the eastern Antarctic plateau. Dust flux in the ice, which is typically measured as the concentration in $\mathbf{(ng\ g^{-1})}$ for soluble dust and particle number concentration in $\mathbf{(P\ ml^{-1})}$ for insoluble dust as a function of ice core depth, is generally sensitive to source emissions and atmospheric cleansing, both of which are linked to the characteristics of the hydrological cycle, that is in turn related to sea surface temperature.

This relationship between dust and temperature is nonlinear: it has multiple modes and thresholds with respect to temperature (7). Due to the low accumulation rate in Antarctica and the log-normal distribution of dust proxy data, the logarithmic values of dust flux are generally used for studying the dust-temperature coupling (2), effectively leading to a log-linear model. Typically, the logarithms of dust fluxes and temperature are uncorrelated for warm periods (interglacial mode) and correlated for relatively cold periods (glacial conditions) (7). Several types of correlations are observed depending on temperature thresholds and temporal proximity to glacial terminations (7, 10). These correlations are established using regression analysis methods.

In this chapter, we look beyond the conventional regression analysis techniques by analyzing the statistical nonstationarity in the high-frequency component of logarithmized dust flux. We show that high nonstationarity on certain time intervals may be related to atmospheric reorganizations that are likely to accompany major climatic transitions. In other words, nonstationarity analysis provides new information on the dynamics of past

climate change, which cannot be extracted by regression analysis.

To examine the nonstationarity, we use flicker-noise spectroscopy (FNS), a phenomenological framework for extracting information from time series with stochastically varying components (16, 17, 18). We apply the FNS nonstationarity factor function to identify the time intervals of major rearrangements (within relatively short time intervals) of the complex system under study. The FNS nonstationarity factor was previously used to locate precursors to strong earthquakes (1, 12, 19, 3, 4, 11).

The chapter is structured as follows. Section 1.2 introduces the principles of FNS. Sections 1.3 and 1.4 explain the algorithms for smoothing and evaluating the nonstationarity factor, respectively. Section 1.5 depicts the complete procedure for the nonstationarity analysis of dust flux time series. Section 1.6 briefly describes the experimental data. The results of the analysis and their interpretation are provided in Section 1.7. The main conclusions and directions for future research studies are given in Section 1.8.

1.2 Principles of Flicker-Noise Spectroscopy

Here, we will only deal with the basic FNS relations needed to understand the nonstationarity factor. FNS is described in more detail elsewhere (16, 17, 18, 15, 8).

In FNS, all introduced parameters for signal $V(t)$, where t is time, are related to the autocorrelation function

$$\psi(\tau) = \langle V(t)V(t+\tau)\rangle_{T-\tau}\,, \tag{1.1}$$

where τ is the time lag parameter ($0 < \tau \leq T_M$) and T_M is the upper bound for τ ($T_M \leq T/2$). This function characterizes the correlation in values of dynamic variable V at higher, $t+\tau$, and lower, t, values of the argument. The angular brackets in relation (1.1) stand for the averaging over time interval $[0,\, T-\tau]$:

$$\langle(...)\rangle_{T-\tau} = \frac{1}{T-\tau}\int_0^{T-\tau}(...)\,dt. \tag{1.2}$$

The averaging over interval $[0,\, T-\tau]$ implies that all the characteristics that can be extracted by analyzing functions $\psi(\tau)$ should be regarded as the average values on this interval.

To extract the information contained in $\psi(\tau)$ ($\langle V(t)\rangle = 0$ is assumed), the following transforms, or "projections", of this function are analyzed: cosine

transforms ("power spectrum" estimates) $S(f)$, where f is the frequency,

$$S(f) = 2\int_0^{T_M} \langle V(t)V(t+t_1)\rangle_{T-\tau} \cos(2\pi f t_1)\, dt_1 \tag{1.3}$$

and its difference moments (Kolmogorov transient structure functions) of the second order $\Phi^{(2)}(\tau)$

$$\Phi^{(2)}(\tau) = \left\langle [V(t) - V(t+\tau)]^2 \right\rangle_{T-\tau}. \tag{1.4}$$

Here, we use the quotes for power spectrum because according to the Wiener-Khinchin theorem the cosine (Fourier) transform of autocorrelation function is equal to the power spectral density only for wide-sense stationary signals at infinite integration limits.

The information contents of $S(f)$ and $\Phi^{(2)}(\tau)$ are generally different, and the parameters for both functions are needed to solve parameterization problems. By considering the intermittent character of signals under study, interpolation expressions for the stochastic components ${\Phi_s}^{(2)}(\tau)$ and $S_s(f)$ of $S(f)$ and $\Phi^{(2)}(\tau)$, respectively, were derived using the theory of generalized functions by (14). It was shown that the stochastic components of structure functions $\Phi^{(2)}(\tau)$ are formed only by jump-like irregularities ("random walks"), and stochastic components of functions $S(f)$, which characterize the "energy side" of the process, are formed by spike-like (inertial) and jump-like irregularities.

1.3 FNS Smoothing Procedure

The analysis of experimental stochastic series often requires the original data to be smoothed. In this study, we apply the "relaxation" procedure proposed for nonstationary signals by (13) based on the analogy with a finite-difference solution of the diffusion equation, which allows one to split the original signal into low-frequency $V_R(t)$ and high-frequency $V_F(t)$ components.

Consider the one-dimensional diffusion equation for V_R :

$$\frac{\partial V_R}{\partial \tau} = \chi \frac{\partial^2 V_R}{\partial t^2} \tag{1.5}$$

with symmetric boundary conditions

$$\frac{\partial V_R}{\partial t} = 0 \quad \text{at} \quad t = 0, \tag{1.6}$$

$$\frac{\partial V_R}{\partial t} = 0 \quad \text{at} \quad t = T \tag{1.7}$$

and initial condition

$$V_R(0) = V(t), \tag{1.8}$$

where χ is a constant diffusion coefficient.

Writing a forward difference for the local term and second-order central difference for the diffusion term, Equation (1.5) gets transformed to

$$\frac{V_k^{i+1} - V_k^i}{\Delta\tau} = \chi \frac{V_{k+1}^i - 2\,V_k^i + V_{k-1}^i}{(\Delta t)^2}, \tag{1.9}$$

where i is the "time" index and k is the "spatial" index. Here, the subscript R is dropped for simplicity.

After introducing $\omega = \frac{\chi \Delta\tau}{(\Delta t)^2}$, Equation (1.9) can be further transformed to the following explicit finite difference expression:

$$V_k^{i+1} = \omega\, V_{k+1}^i + (1 - 2\,\omega\,)\, V_k^i + \omega\, V_{k-1}^i. \tag{1.10}$$

Analogously, the finite difference formulation for the complete problem (1.5)–(1.9) can be written as

$$V_1^{i+1} = (1 - 2\,\omega\,)\, V_1^i + 2\omega V_2^i, \tag{1.11}$$

$$V_k^{i+1} = \omega V_{k+1}^i + (1 - 2\,\omega\,)\, V_k^i + \omega V_{k-1}^i, \tag{1.12}$$

$$V_{N_t}^{i+1} = (1 - 2\,\omega\,)\, V_{N_t}^i + 2\omega V_{N_t-1}^i. \tag{1.13}$$

Here, i is the current iteration number and N_t is the length of the time series. The smoothing procedure (1.11)–(1.13) is unconditionally stable for $\omega < 1/2$, which is the maximum allowed value for ω in the smoothing algorithm. There are two input parameters: the number of iterations i_{max} (largest value for i), which is equivalent to a certain "cutoff" frequency for the time series under study, and the value for ω. Expressions (1.11)–(1.13) are evaluated at each iteration.

In summary, the smoothing procedure finds new values of the signal at every "relaxation" step using its values for the previous time step, yielding the low-frequency component V_R at the end. The high-frequency component V_F is obtained by subtracting V_R from the original signal. Conceptually speaking, this algorithm progressively reduces the local gradients of the "concentration" variable, causing the points in every triplet to come closer to each other.

1.4 FNS Nonstationarity Factor

To analyze the effects of nonstationarity in real processes, we study the dynamics of changes in $\Phi^{(2)}(\tau)$ for consecutive "window" intervals $[t_k, t_k+T]$, where $k = 0, 1, 2, 3, ...$ and $t_k = k\Delta T$, that are shifted within the total time interval T_{tot} of experimental time series ($t_k + T < T_{tot}$). The averaging interval T and difference ΔT are chosen based on the physical understanding of the problem in view of the suggested characteristic time of the process, which is the key parameter of system evolution.

The FNS nonstationarity factor $C_J(t_k)$ is defined as

$$C_J(t_k) = 2 \cdot \frac{Q_k^J - P_k^J}{Q_k^J + P_k^J} \cdot \frac{T}{\Delta T}, \tag{1.14}$$

$$Q_k^J = \frac{1}{\alpha T^2} \int_0^{\alpha T} \int_{t_k}^{t_k+T} [V_J(t) - V_J(t+\tau)]^2 \, dt \, d\tau, \tag{1.15}$$

$$P_k^J = \frac{1}{\alpha T^2} \int_0^{\alpha T} \int_{t_k}^{t_k+T-\Delta T} [V_J(t) - V_J(t+\tau)]^2 \, dt \, d\tau. \tag{1.16}$$

Here, J indicates which function $V_J(t)$ ($J = R$, F or G) is used, and the subscripts R, F, and G refer to the low-frequency (regular) component, high-frequency (fluctuation) component, and unfiltered signal, respectively. Note that the integrands in Eqs. (1.15)–(1.16) correspond to the structural function $\Phi_J^{(2)}(\tau)$ given by Eq. (1.4).

The FNS nonstationarity factor in discrete for is written as ($b = \lfloor \Delta T/\Delta t \rfloor$, $N_1 = \lfloor \alpha N \rfloor$):

$$C_J(t_k) = 2 \cdot \frac{Q_k^J - P_k^J}{Q_k^J + P_k^J} \Big/ \frac{\Delta T}{T}, \tag{1.17}$$

$$Q_k^J = \frac{1}{N_1} \sum_{n_\tau=1}^{N_1} \frac{1}{N - n_\tau} \sum_{m=1+kb}^{N-n_\tau+kb} [V_J(m) - V_J(m+n_\tau)]^p, \tag{1.18}$$

$$P_k^J = \frac{1}{N_1} \sum_{n_\tau=1}^{N_1} \frac{1}{N - n_\tau} \sum_{m=1+kb}^{N-n_\tau+(k-1)b} [V_J(m) - V_J(m+n_\tau)]^p. \tag{1.19}$$

Note that functions $\Phi_J^{(2)}(\tau)$ can be reliably evaluated only on the τ interval of $[0, \alpha T]$ that is less than half the averaging interval T; i.e., $\alpha < 0.5$.

In earthquake prediction studies, the phenomenon of "precursor" occurrence is assumed to be related to abrupt changes in functions $\Phi^{(2)}(\tau)$ when the upper bound of the interval $[t_k, t_k + T]$ approaches the time moment t_c of a catastrophic event accompanied by total system reconfiguration on all space scales. Graphically, this corresponds to peaks in the plots of nonstationarity factor.

1.5 Experimental Data

The EPICA Dome C ice core was drilled in East Antarctica (75°06′ S; 123°21′ E) and covers the last 800,000 years (5). From a depth of 24.2m down to 3200m, a Continuous Flow Analysis (CFA) system (9) was applied to measure, among others, Ca^{2+}, Na^{+}, and dust particles. The data gathered with this method have a nominal depth resolution of ∼1 cm, taking dispersion in the CFA system into account, which corresponds to a formal sub-annual temporal resolution at the top and up to ∼25 years at the bottom of the ice core. Practically, surface snow mixing and dispersion in the ice result in a lower effective temporal resolution.

In this study, we examine the dust flux time series derived using the principal component analysis of three complete datasets recorded at the EPICA Dome C ice core: soluble Ca^{2+} and non-sea-salt Ca^{2+} concentrations, as well as insoluble dust particle numbers (6). This dataset, hereafter referred to as PC1, was calibrated to dust mass flux units using a two-sided regression analysis between PC1 and dust flux measurements from standard Coulter Counter analysis. More detailed description is provided elsewhere (6).

1.6 Procedure for Analysis

The PC1 time series contains several small gaps (generally not exceeding few sampling points). These missing values were estimated using a linear interpolation between the values adjacent to the gap. Then the time series was ordered chronologically (instead of the standard order by age used in paleoclimatology). The PC1 dust flux values were next logarithmized (due to the low accumulation rate in Antarctica and the log-normal distribution of dust proxy data) to study its correlation with temperature. As a first step, we applied a moving average operation to the time series using 5-point subsets to minimize the effect of single-point spikes. The low-frequency part of the PC1

dust flux is dominated by orbital frequencies (due to eccentricity, obliquity, and precession parameters of Earth's orbit around the Sun) and not relevant to high-frequency changes in Earth's atmosphere. It was therefore excluded using the FNS smoothing procedure (see chapter 1.3), in which we chose the number of iterations i_{max} in such a way that it corresponds to an effective "cuttoff" frequency of $(5 \text{ kyr})^{-1}$. Finally, the nonstationarity factors C_F for different values of averaging interval T were computed, and the resulting time series were reordered by age.

To estimate the significance thresholds corresponding to background noise, the same procedure that was applied to the logarithmized dataset of PC1 was performed for synthetic Gaussian noise (in view of the fact that the power spectrum estimate for the high-frequency component of logarithmized dust flux has a slope relatively close to 0). The histogram of C_F for Gaussian noise was then fitted to the Burr distribution (FNS nonstationarity factor generally has a skewed asymetric distribution that can be well-approximated by the Burr distribution). The 95% and 97.5% significance thresholds were computed for the Gaussian noise signal using the cumulative distribution function. The ratio of the count of values above the threshold for PC1 to the count for Gaussian noise was calculated to check the statistical significance.

1.7 Results and Discussion

Figures 1.1 and 1.2 illustrate the time series for temperature (5), logarithmized PC1, and its low-frequency and high-frequency components for the last 800 kyr and 100 kyr, respectively. It can be seen that temperature and logarithmized PC1 (as well as its low-frequency part) are generally anticorrelated for glacial (low temperature) intervals. During interglacial intervals (highest temperatures), temperature and logarithmized PC1 are much less correlated. This relationship can be examined by regression methods and is discussed in detail elsewhere (7).

Our focus is on the behavior of the high-frequency component, which in this case includes the frequencies between $\sim (5,000 \text{ yr})^{-1}$ and $\sim (50 \text{ yr})^{-1}$. The lower frequency bound corresponds to the "cutoff" for the FNS smoothing procedure, and the upper frequency bound is obtained as a result of applying the moving average procedure on 5-point subsets. Although it is hard to see any direct correlations between temperature and the high-frequency component of logarithmized PC1, one can observe some apparent nonstationarity in the high-frequency component displayed in Fig. 1.1. This nonstationarity can be examined using the FNS nonstationarity factor.

Figures 1.3 and 1.4 show temperature along with the nonstationarity fac-

Figure 1.1: Temperature, logarithmized dust flux at EPICA Dome C, and its low-frequency and high-frequency components for the last 800 kyr.

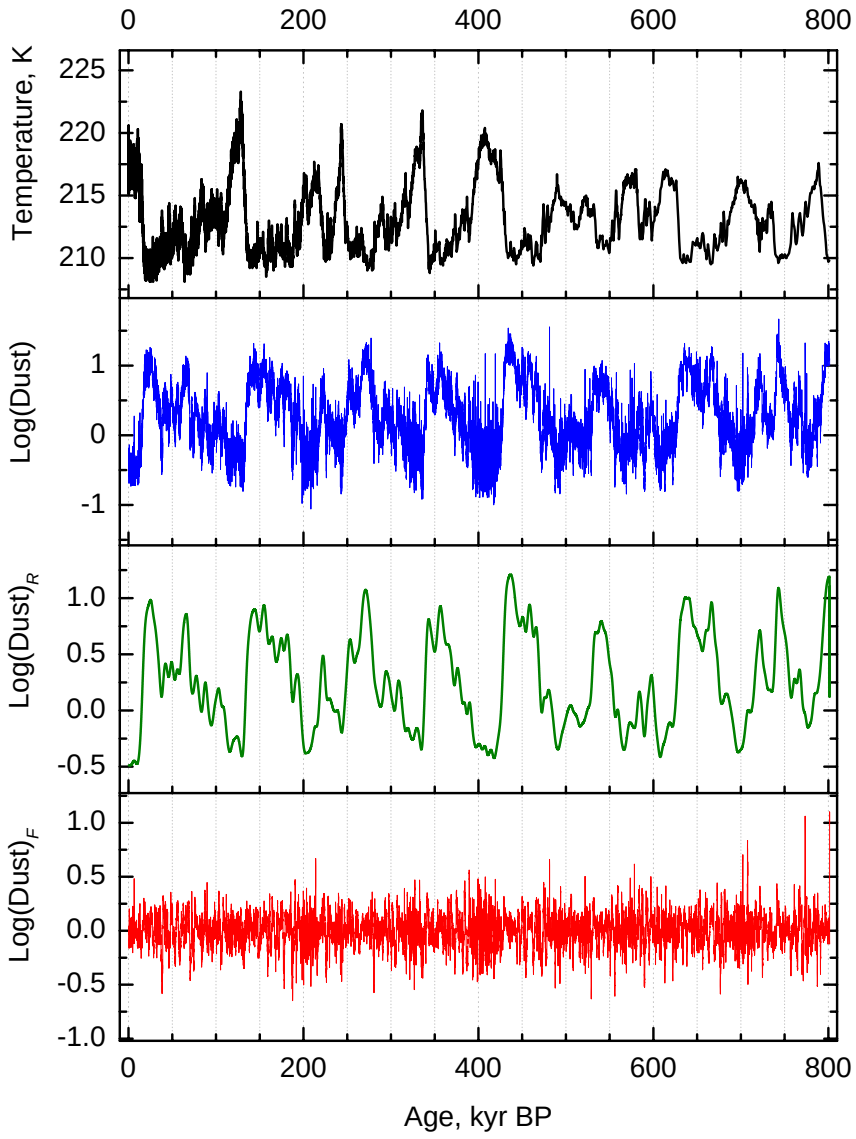

Figure 1.2: Temperature, logarithmized dust flux at EPICA Dome C, and its low-frequency and high-frequency components for the last 100 kyr.

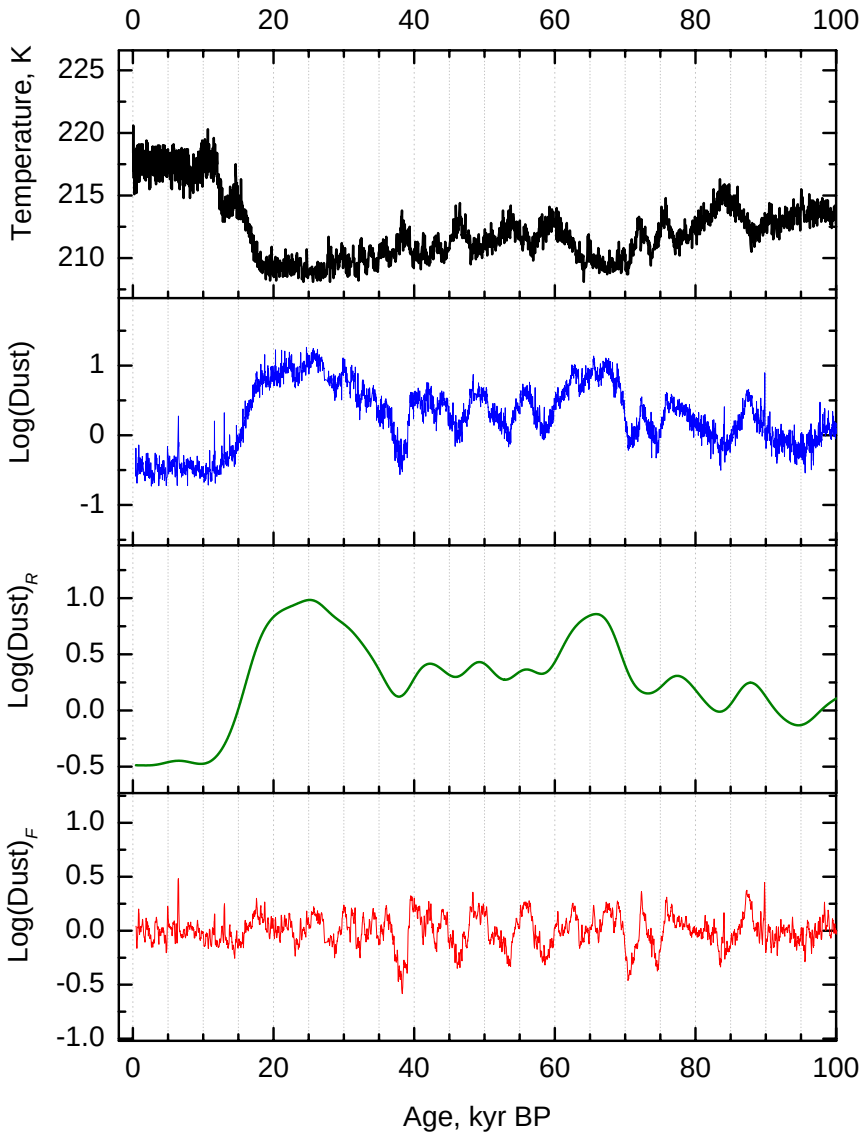

tor for the high-frequency component of logarithmized PC1 at the averaging intervals of 12.5, 25, and 37.5 kyr for the last 800 kyr and 100 kyr, respectively. Each plot for nonstationarity factor C_F also displays two thresholds, 95% (lower) and 97.5% (upper), estimated using the analysis of the nonstationarity factor for Gaussian noise in terms of the Burr distribution. The value of the 95% threshold for C_F is 3.80–3.84 for all three values of the averaging intervals. The values for the 97.5% threshold lie in the range from 5.70 to 5.76. The ratios of the count of points above the 95% threshold for PC1 to the count for Gaussian noise are 1.67:1, 1.40:1, and 1.29:1 for T=12.5, 25, and 37.5 kyr, respectively. In the case of the 97.5% threshold, the ratios are 2.91:1, 2.52:1, and 2.12:1, respectively. The highest values of the ratio correspond to the smallest averaging interval (12.5 kyr).

Figure 1.3 shows that higher values of the averaging interval T lead to more non-uniform distribution of nonstationarity factor. There are intervals of high activity along with quiescent intervals. The plot for T = 37.5 kyr demonstrates that quiescent intervals correspond to glacial conditions while the intervals of high activity appear to happen when substantial warming is observed. Physically, this may imply that glacial climate is generally stable until some perturbation (warming) occurs. The perturbation may grow into a large-scale instability, possibly associated with an atmospheric reorganization at multiple scales. This allows us to explain why when the climate system is stable, clear anticorrelations between temperature and logarithmized dust are observed; and then when the climate system becomes unstable, the correlations start to disappear (7).

Figure 1.4 illustrates the intermittence between quiescent and active periods in the plots of nonstationarity factor C_F for the last 100 kyr. For instance, there is a quiescent interval in the C_F plots between 20 kyr and 38 kyr before present (BP) for all values of T, which coincides with full glacial conditions (temperature values do not exceed 212 K). However, there are elevated levels of nonstationarity in the C_F plot between 60 and 38 kyr BP, which corresponds to a period with large temperature variations. Especially during the last glacial-interglacial transition (10-20 kyr BP), it can be seen that C_F at T=12.5 kyr is most informative. In this case it is due to the fact that the time scale of individual features (climatic events) in the plot of temperature is much smaller for the interval from 0 to 100 kyr BP (Fig. 1.4) as compared to the range from 0 to 800 kyr BP (Fig. 1.3). If one looks at a more granular level, the values of the averaging interval should be further reduced to a level comparable to the characteristic time-scale of observed climatic events.

Figure 1.3: Temperature and nonstationarity factor for the high-frequency component of logarithmized PC1 at the averaging intervals of 12.5, 25, and 37.5 kyr for the last 800 kyr. Horizontal lines in each plot for C_F correspond to 95% (lower) and 97.5% (upper) thresholds for Gaussian noise.

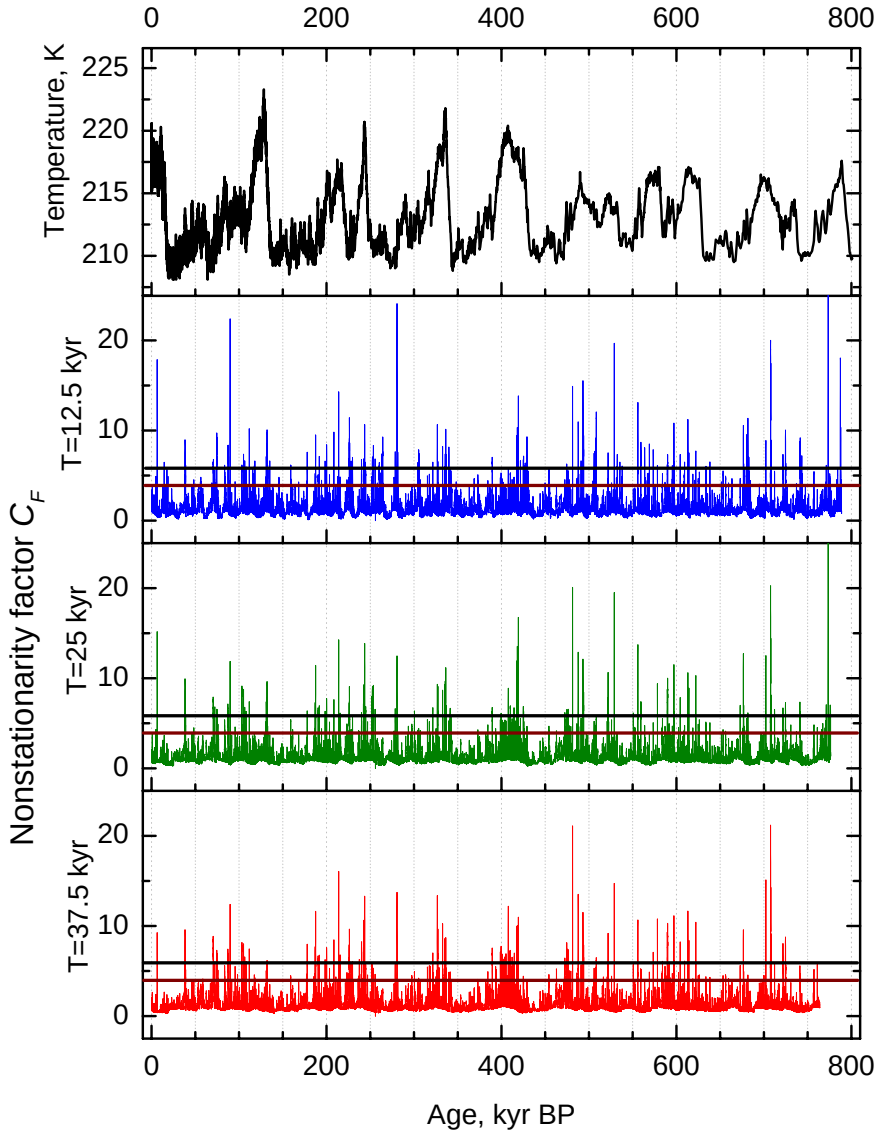

Figure 1.4: Temperature and nonstationarity factor for the high-frequency component of logarithmized PC1 at the averaging intervals of 12.5, 25, and 37.5 kyr for the last 100 kyr. Horizontal lines in each plot for C_F correspond to 95% (lower) and 97.5% (upper) thresholds for Gaussian noise.

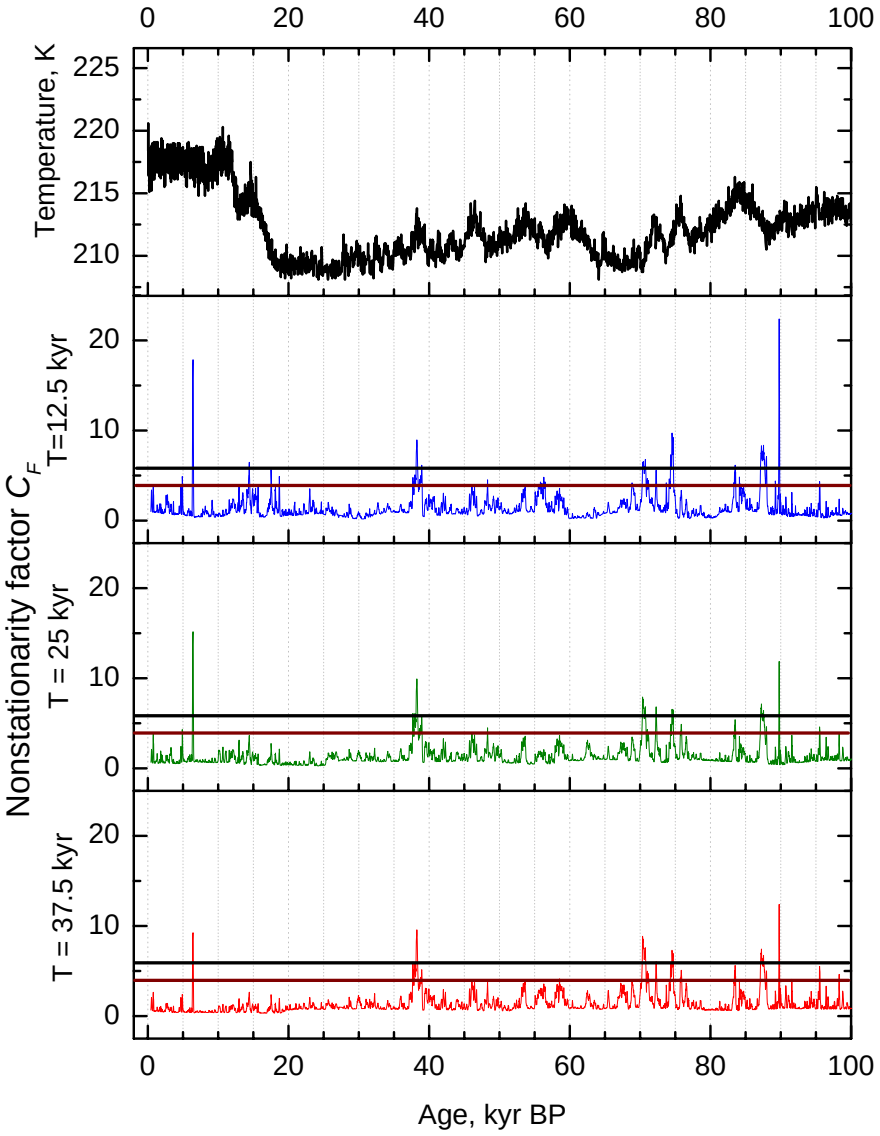

1.8 Concluding Remarks

Our study shows that the dust flux time series derived from the EPICA Dome C ice core data is statistically nonstationary. It contains alternating intervals of quiescence and high activity. The quiescent intervals appear to be related to cold conditions in the temperature series (5), whereas periods of high activity seem to correspond to warming events, potentially leading to interglacial conditions. It is generally thought there is a significant correlation between dust flux and temperature records during glacial periods and virtually no correlation during interglacial periods (7). Our results suggest that the climate system is stable during cold times (quiescent intervals), which is why the correlation is observed. Conversely, the climatic system seems to be perturbed by warming and lose its stability (high activity intervals), thus breaking down the causal link between Southern Hemisphere surface temperature and dust flux in Antarctica.

The main goal of this study is to demonstrate that nonstationarity analysis and particularly the FNS nonstationarity factor may provide new information in the analysis of loglinear models used in paleoclimatology. This information cannot be acquired using regression methods but may explain why certain correlations are present or absent. The information from nonstationarity analysis may also help in developing climate models that study the onset of unstable climatic modes. To form a more complete picture of how nonstationary processes in atmospheric signals interact with temperature, it is necessary to study other climate proxies for Antarctica as well as other geographic regions. One would also need to analyze the time series at different scales (using different values of the averaging interval in evaluating the FNS nonstationarity factor) and examine the behavior for various glacial-interglacial climatic cycles, as well as millennial-scale oscillations in both hemispheres.

References

1. A. V. Descherevsky, A. A. Lukk, A. Y. Sidorin, G. V. Vstovsky, and S. F. Timashev. Flicker-noise spectroscopy in earthquake prediction research. *Nat. Hazards Earth Syst. Sci.*, 3:159–164, 2003.
2. H. Fischer, M.-L. Siggaard-Andersen, U. Ruth, R. Rthlisberger, and E. Wolff. Glacial/interglacial changes in mineral dust and sea-salt records in polar ice cores: Sources, transport, and deposition. *Reviews of Geophysics*, 45(1):RG1002, 2007.

3. M. Hayakawa and S. F. Timashev. An attempt to find precursors in the ulf geomagnetic data by means of flicker noise spectroscopy. *Nonlinear Proc. Geophys.*, 13(3):255–263, 2006.

4. Y. Ida, M. Hayakawa, and S. Timashev. Application of different signal analysis methods to the ulf data for the 1993 guam earthquake. *Nat. Hazards Earth Syst. Sci.*, 7(4):479–484, 2007.

5. J. Jouzel, V. Masson-Delmotte, O. Cattani, G. Dreyfus, S. Falourd, G. Hoffmann, B. Minster, J. Nouet, J. M. Barnola, J. Chappellaz, H. Fischer, J. C. Gallet, S. Johnsen, M. Leuenberger, L. Loulergue, D. Luethi, H. Oerter, F. Parrenin, G. Raisbeck, D. Raynaud, A. Schilt, J. Schwander, E. Selmo, R. Souchez, R. Spahni, B. Stauffer, J. P. Steffensen, B. Stenni, T. F. Stocker, J. L. Tison, M. Werner, and E. W. Wolff. Orbital and millennial antarctic climate variability over the past 800,000 years. *Science*, 317(5839):793–796, 2007.

6. F. Lambert, M. Bigler, J. P. Steffensen, M. Hutterli, and H. Fischer. Centennial mineral dust variability in high-resolution ice core data from dome c, antarctica. *Climate of the Past*, 8(2):609–623, 2012.

7. F. Lambert, B. Delmonte, J. R. Petit, M. Bigler, P. R. Kaufmann, M. A. Hutterli, T. F. Stocker, U. Ruth, J. P. Steffensen, and V. Maggi. Dust-climate couplings over the past 800,000 years from the epica dome c ice core. *Nature*, 452:616–619, 2008.

8. Y. S. Polyakov, J. Neilsen, and S. F. Timashev. Stochastic variability in x-ray emission from the black hole binary GRS 1915+105. *Astron. J.*, 143(6):148, 2012.

9. R. Röthlisberger, M. Bigler, M. Hutterli, S. Sommer, B. Stauffer, H. G. Junghans, and D. Wagenbach. Technique for continuous high-resolution analysis of trace substances in firn and ice cores. *Environmental Science and Technology*, 34(2):338–342, 2000.

10. R. Röthlisberger, M. Mudelsee, M. Bigler, M. de Angelis, H. Fischer, M. Hansson, F. Lambert, V. Masson-Delmotte, L. Sime, R. Udisti, and E. W. Wolff. The southern hemisphere at glacial terminations: insights from the dome c ice core. *Climate of the Past Discussions*, 4(3):761–789, 2008.

11. G. V. Ryabinin, Y. S. Polyakov, V. A. Gavrilov, and S. F. Timashev. Identification of earthquake precursors in the hydrogeochemical and geoacoustic data for the kamchatka peninsula by flicker-noise spectroscopy. *Natural Hazards and Earth System Science*, 11(2):541–548, 2011.

12. L. Telesca, V. Lapenna, S. Timashev, G. Vstovsky, and G. Martinelli.

Flicker-noise spectroscopy: a new approach to investigate the time dynamics of geoelectrical signals measured in seismic areas. *Phys. Chem. Earth.*, 29:389–395, 2004.

13. S. Timashev and G. Vstovskii. Flicker-noise spectroscopy for analyzing chaotic time series of dynamic variables: Problem of signal-to-noise relation. *Russ. J. Electrochem.*, 39(2):141–153, 2003.
14. S. F. Timashev. Flicker noise spectroscopy and its application: Information hidden in chaotic signals. *Russ. J. Electrochem.*, 42:424, 2006.
15. S. F. Timashev, O. Y. Panischev, Y. S. Polyakov, S. A. Demin, and A. Y. Kaplan. Analysis of cross-correlations in electroencephalogram signals as an approach to proactive diagnosis of schizophrenia. *Physica A*, 391(4):1179, 2012.
16. S. F. Timashev and Y. S. Polyakov. Review of flicker noise spectroscopy in electrochemistry. *Fluct. Noise Lett.*, 7:R15–R47, 2007.
17. S. F. Timashev and Y. S. Polyakov. Analysis of discrete signals with stochastic components using flicker noise spectroscopy. *Int. J. Bifurcation Chaos*, 18:2793–2797, 2008.
18. S. F. Timashev, Y. S. Polyakov, P. I. Misurkin, and S. G. Lakeev. Anomalous diffusion as a stochastic component in the dynamics of complex processes. *Phys. Rev. E*, 81:041128–1–041128–17, 2010.
19. G. V. Vstovsky, A. V. Descherevsky, A. A. Lukk, A. Y. Sidorin, and S. F. Timashev. Search for electric earthquake precursors by the method of flicker-noise spectroscopy. *Izv.-Phys. Soild Earth*, 41:513–524, 2005.